MDPI

Article

Design and Construction of a Laboratory-Scale Direct-Current Electric Arc Furnace for Metallurgical and High-Titanium Slag Smelting Studies

Botao Xue [1], **Lingzhi Yang** [1,*], **Yufeng Guo** [1], **Feng Chen** [1], **Shuai Wang** [1], **Fuqiang Zheng** [1] **and Zeshi Yang** [2]

[1] School of Minerals Processing and Bioengineering, Central South University, Changsha 410083, China; xuebotao@csu.edu.cn (B.X.); yfguo@csu.edu.cn (Y.G.); csuchenf@csu.edu.cn (F.C.); wang_shuai@csu.edu.cn (S.W.); f.q.zheng@csu.edu.cn (F.Z.)

[2] Department of Mechanical Engineering, National University of Singapore, Singapore 117575, Singapore; yangzeshi@n.nus.edu

* Correspondence: yanglingzhi@csu.edu.cn; Tel.: +86-159-7413-1987

Abstract: A novel direct-current electric arc furnace (DC-EAF) was designed and constructed in this study for experimentally investigating high-titanium slag smelting, with an emphasis on addressing the issues of incomplete separation of metal and slag as well as poor insulation effects. The mechanical components (crucible, electrode, furnace lining, etc.) were designed and developed, and an embedded crucible design was adopted to promote metal-slag separation. The lining and bottom thicknesses of the furnace were determined via calculation using the heat balance equations, which improved the thermal insulation. To monitor the DC-EAF electrical parameters, suitable software was developed. For evaluating the performance of the furnace, a series of tests were run to determine the optimal coke addition under the conditions of constant temperature (1607 °C) and melting time (90 min). The results demonstrated that for 12 kg of titanium-containing metallized pellets, 4% coke was the most effective for enrichment of TiO_2 in the high-titanium slag, with the TiO_2 content reaching 93.34%. Moreover, the DC-EAF met the design requirements pertaining to lining thickness and facilitated metal-slag separation, showing satisfactory performance during experiments.

Keywords: DC electric arc furnace; high-titanium slag; mechanical design; PLC data collection; software development

1. Introduction

Electric arc furnace (EAF) smelting generates an electric arc between the graphite electrode and the metal in the furnace, and it employs the thermal effect of the electric arc for heating and melting the metal to produce high-quality products [1,2]. In China, only large capacity industrial EAFs (over 30 t) have been retained to accelerate capacity replacement and reduce production costs since 2016 [3]. The structure of these industrial EAFs is highly complex [2,4], which makes it inconvenient and uneconomical for many research institutions and universities to use them for metallurgical experiments due to the high costs of the experiments.

With economic development and suitable policy framing, the development of laboratories in universities and scientific research institutions has progressed significantly, and the investment in scientific research infrastructure, such as developing advanced equipment and materials for metallurgy-based research, has increased. Herein, we review the history of DC-EAF development. In the early 1970s, Swiss's Asea Brown Boveri (ABB) group designed and developed a seven-ton EAF and carried out a large number of tests on it. In 1979, the CLECIM Company built a six-ton and 4.5 MW DC-EAF (where DC is direct-current) for steel production. In 1985, the MAN Gutehoffnungshutte (MAN-GHH) group in Germany built a half-ton EAF. In 1991, the Chengdu Seamless Steel Tube Company built the first five-ton DC-EAF for steelmaking in China [5,6]. In 2007, Festus et al.

constructed an EAF that could melt approximately 5 kg of scrap steel. Tests showed that heating the furnace to the melting temperature (1150–1400 °C) of the cast iron takes a considerable amount of time [7]. In 2011, Yin et al. used a 50 kVA DC-EAF for studying water-quenched slag. In the experiment, the actual power of the equipment was low, the temperature could only be maintained at 1400 ± 30 °C, the operation was unstable, and tripping was severe [8]. In 2015, Barbouche et al. developed a small DC-EAF for metallurgical experimental research and collected temperature and flow data via computer control. However, the device is small, which is not conducive to expanding its application [9]. In, the aforementioned experimental EAF smelting methods, secondary mixing of molten steel and steel slag, especially in the pouring process of molten steel in the tilting furnace, is a common problem and therefore the metal and slag cannot be completely separated. A variety of tapping methods were used in these DC-EAF studies, as shown in Table 1.

Table 1. Comparison of the tapping methods in Previous Studies.

Company	Year	Capacity	Note	References
ABB	1972	7 t	\	Sun et al. [10]
IRSID	1979	6 t	\	Xu [5]
MAN-GHH	1982	12 t	Bottom tapping	Schub., M et al. [11]
SMS	1983	12 t	Tilting tapping	Gu [12]
MAN-GHH	1985	0.5 t	\	Xu [5]
Taiyuan Heavy Machinery	1989	5 t	Tilting tapping	Zhang [13]
Chengdu Seamless Steel Tube	1991	5 t	Tilting tapping	Wang et al. [14]
Shanghai Fifth Steel Works	1995	10 t	EBT	Liu [15]
\	2007	2 kg	Tilting tapping	Festus et al. [7]
\	2011	250 kg	Tilting tapping	Yin et al. [8]
\	2015	\	\	Barbouche et al. [9]

In this study, a small DC-EAF was designed for the direct reduction of titanium-containing metallized pellets to the separation of slag and iron, and to obtain molten iron and high-titanium slag. This involved the design and construction of the mechanical structure, followed by electrical design and software development. The mechanical aspect includes the design of the furnace size and lining, as well as reasonable modification of the crucible to effectively separate the metal and slag. A programmable logic controller (PLC) was used to collect data to ensure the accuracy and reliability of the data. Accordingly, a process monitoring system was developed. Our primary objective was to design a small DC-EAF for melting separation experimental research. Our results show that DC-EAF achieves a good separation effect of metal slag and had satisfactory performance during experimentation, thus, highlighting its potential application in industry.

2. Theoretical Design and Calculation

Titanium dioxide is an important inorganic chemical material, which is widely used in coating, papermaking, rubber, chemical fiber, and other industries. It has been widely used in industry, agriculture, and national defense [16]. Because of the low titanium content in China's titanium resources, the primary titanium ore cannot be directly used to produce titanium dioxide, and the method of smelting titanium slag must be used to meet the needs. Usually, the EAF is used to heat and melt ilmenite, so that the high-content enrichment of TiO_2 is obtained after the separation of TiO_2 and iron in ilmenite. The raw materials are ilmenite and carbon according to the following chemical reaction [17]:

$$FeTiO_3 + C \rightarrow TiO_2 + Fe + CO \tag{1}$$

Electric arc furnaces (EAFs) have numerous properties required in furnaces for metallurgical and ilmenite research. Such features include local temperature and heat control, accurate analysis of melting, definite metal refining sequence, and high thermal efficiency (as high as 70%) [18].

2.1. Electrical Conception

2.1.1. Selection of Power Supply

Compared with AC-EAFs (where AC is alternating-current), DC-EAFs have lower electrode consumption, more uniform temperature distribution, a simple structure, higher economic benefit, and are more suitable for metallurgical research in colleges and universities [19–21]. The design of the DC-EAF is shown in Figure 1. A single-electrode DC tilting furnace-type is adopted; that is, a three-phase DC power is obtained as the output after rectification. The furnace bottom is connected to one pole of the power source, and the graphite electrode on the upper side is connected to the other pole.
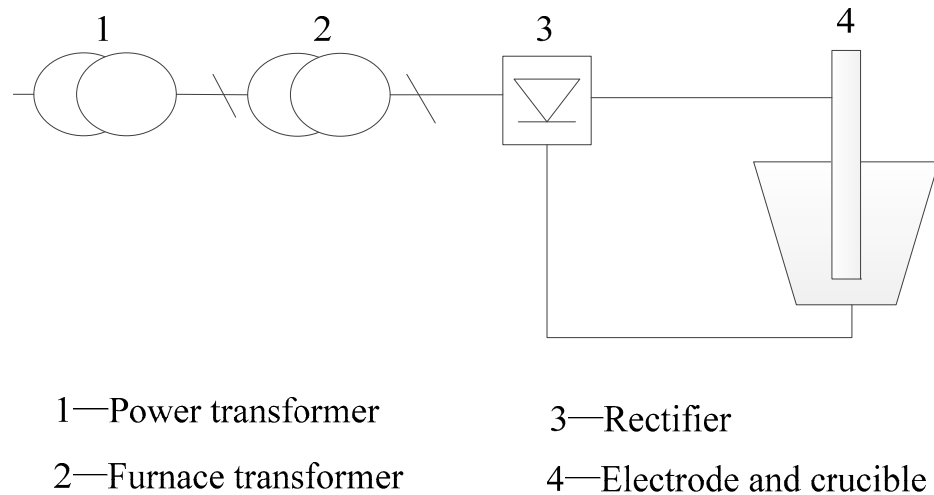

1—Power transformer　　　　3—Rectifier

2—Furnace transformer　　　4—Electrode and crucible

Figure 1. Schematic diagram of the electric arc furnace system structure.

2.1.2. Electrode and Holder Design

The electrode carries the current to the molten pool. Current passing through the electrode generates heat. The size of the electrode diameter is closely related to the heat energy loss. [7,22]. The suitable diameter, for minimized heat loss, can be calculated using Equation (2).

$$d_{electrode} = \sqrt[3]{\frac{0.406 I^2 \rho}{K}} \tag{2}$$

where $d_{electrode}$ is the diameter of the electrode (cm); I is the average electrical current (A), $I = 500$ A; ρ is resistivity of the electrodes, $\rho = 8$–13 Ω mm^2·m^{-1}; and K is a coefficient (for graphite electrodes, $K = 2.1 \times 10^4$ W·m^{-2}).

The electrode holders are used to hold the electrodes and provide a pathway for current flow. Therefore, red copper material was chosen owing to its good electric conductivity. A 3D drawing of the holder is illustrated in Figure 2.

2.1.3. Electrical Control Design

The basic ideas of the electrical design are described in this section, including the relevant electrical design specifications and safe operation characteristics, by referring to the mechanical and electrical properties of the products, which are used to design the hardware of the DC-EAF [23]. This mainly includes drawing electrical schematic diagrams, wiring equipment, and writing control programs.

The PLC is an important component in the electrical design of an EAF. Thus far, PLCs have been widely used in the industrial sector [24]. Their remarkable characteristics include efficient working in harsh environments (for example, in high-temperature or high-humidity environments) and higher operating speeds than electromechanical control systems [25]. There are numerous ways to increase the arc intensity during the arc furnace melting process. In our experiment, the Siemens s7-200 PLC was used to control the motor and adjust the height of the electrode, such that the strength of the arc can be varied.

Figure 3 shows a schematic diagram of the electrical control system, which helps in heat transmission, from arc to metal, and improves heat assimilation [26]. In addition, the water pump and dust motor were also controlled by the s7-200 PLC.
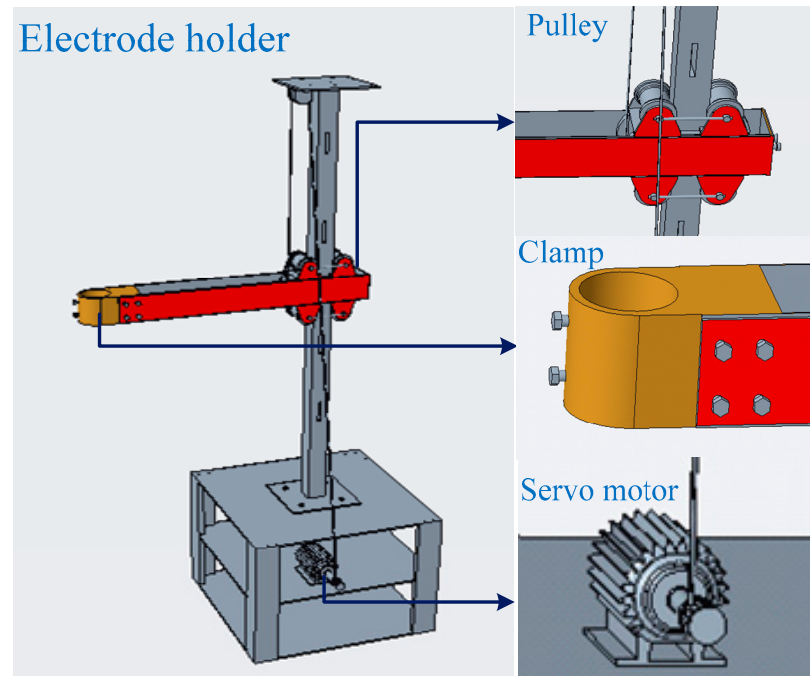

Figure 2. 3D schematic diagram of the electrode holder.
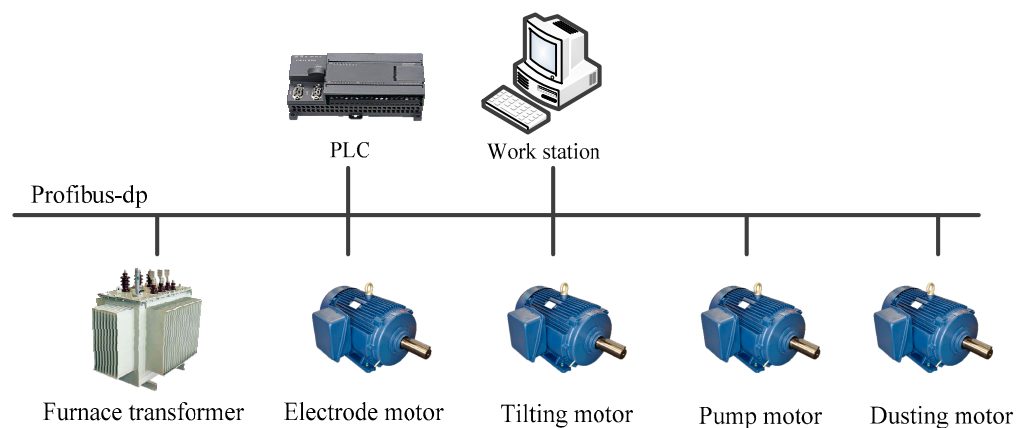
Figure 3. Schematic diagram of the electrical control system.

The PLC control must be programmed on a computer equipped with STEP 7-micro/WIN development tools [27]. The program mainly includes coded instructions to perform electrode lifting, water pump operation, and control the dust removal motor. Real-time data communication is established between the personal computer and the PLC through a TCP/IP protocol [28]. The electrical principle of the EAF, designed according to the national electrical industry design standards combined with laboratory conditions [29,30], is shown in Figure 4.

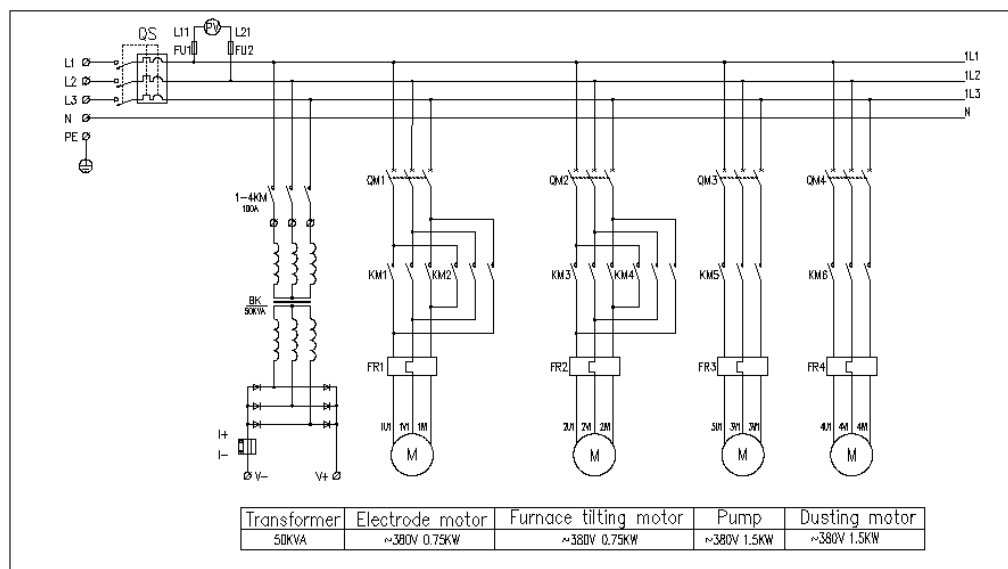**Figure 4.** Schematic diagram of part of the system hardware circuit.

2.2. Mechanical Design

2.2.1. Crucible and Reaction Chamber Design

The shape of the EAF bath must be conducive to the smooth progress of the melting reaction. The crucible, used in this experiment, has a spherical convex top, is shown inFigure 5. This shape of the crucible enables the liquid metal to be deposited at the bottom of the bath, thereby quickly forming a molten pool, which is more convenient when tapping. Finally, graphite crucibles, which show high temperature resistance (above 2000 °C), corrosion resistance, and good electrical conductivity, are selected according to the calculated size, and based on the products available on the market, such that they do not introduce impurities in the smelting materials.

h_3:Furnace top height
H_1:Reaction chamber height
H:Crucible depth
D:Crucible inside diameter
D_r:Reaction chamber diameter
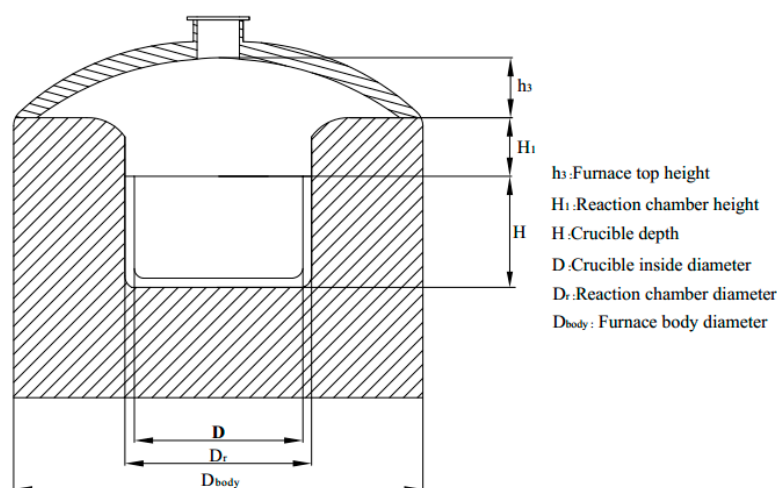D_{body}: Furnace body diameter

Figure 5. Schematic diagram of the arc furnace with dimensions.

The total volume of the crucible can be calculated using Equation (3):

$$V = \frac{\pi}{4}HD^2 \qquad (3)$$

where V is the volume, H is the height, and D is the diameter of the furnace.

The reaction chamber refers to the volume from the molten pool up to the top of the furnace (Figure 5). To prevent the liquid metal from splashing, the diameter of the reaction chamber must be larger than the bath, and is generally calculated using Equation (4):

$$D_r = D + 2\varepsilon \tag{4}$$

where D_r is the diameter of the melting chamber (m), and ε is the thickness of the crucible.

The height of the reaction chamber (H_1) and the height of the furnace top (h_3) are usually determined from the heat exchange in the furnace [18], as shown in Equations (5) and (6):

$$H_1 = 0.42 \times D \tag{5}$$

$$h_3 = \frac{D_r}{2} \tag{6}$$

While dumping the smelted products, the slag is drawn into the liquid metal, which affects the quality of the smelting products, as shown in Figure 6.
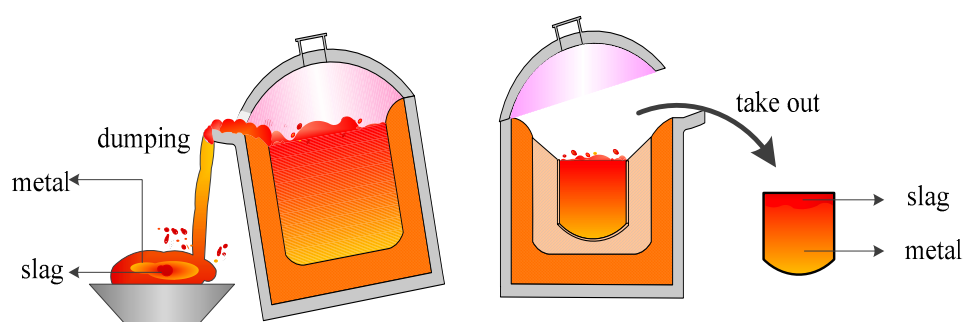

Figure 6. Comparison of metal and slag separation effects.

Further, with increasing smelting times, the complex environment inside the furnace accelerates the erosion (carbon consumption) of the crucible inner wall; however, frequent replacement of the crucible, due to these factors, results in high maintenance costs. Therefore, in our case, a small movable crucible was placed in a large crucible for smelting. After smelting, the product solidified, and the crucible was removed and smashed to obtain the product. This process can effectively prevent the mixing of slag and liquid metal during the dumping process and thus, crucible degradation, thereby mitigating the high maintenance costs.

Figure 7 shows the improved molten pool structure and the physical shape of the small crucible. To ensure good electrical conductivity between two crucibles, a layer of graphite powder is included between them. The surrounding environment is filled with high temperature-resistant asbestos to prevent rapid heat loss. The molten product may be removed when the melting is complete and the crucible cools in the furnace.
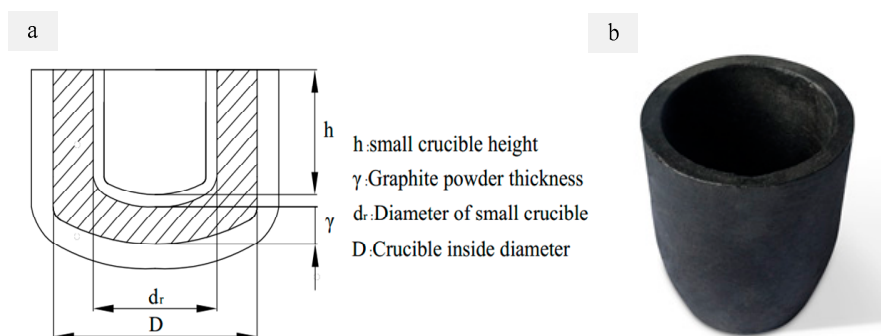

h : small crucible height
γ : Graphite powder thickness
d_r : Diameter of small crucible
D : Crucible inside diameter

Figure 7. (**a**) Schematic diagram and (**b**) image of the improved crucible and molten pool structure.

2.2.2. Furnace Lining Design

In the EAF smelting process, the lining effectively controls the heat loss and ensures uniform heating rate and maximum temperature inside the furnace; thus, the lining and bottom thickness should be rationally designed to ensure that the melting pool temperature reaches 1500–1700 °C within an hour, and the temperature of the furnace outer wall does not exceed 200 °C. To meet these conditions, the theoretical thickness of the furnace bottom and lining is calculated using the formula of a uniform flat wall and cylindrical wall [2], as shown in Equations (7) and (8) below:

$$E^o_{bottom} = \frac{\lambda_b}{\delta_{bottom}}(T_h - T_n) \tag{7}$$

$$E^o_{lining} = \frac{2\pi \times \lambda_l \times L}{ln(d_2/d_1)} \times (T_h - T_n) \tag{8}$$

where E^o_{bottom} is the energy loss at the bottom (W·m^{-2}); E^o_{lining} is the energy loss from the lining (W); t_h is the bath temperature (°C), T_h = 1923 K; t_n is the outer wall temperature (°C) T_n = 473 K, δ_{bottom} is the bottom thickness (m); λ_b is the average thermal conductivity of the furnace bottom (W m^{-1} K^{-1}); λ_l is the average thermal conductivity of the furnace lining (W m^{-1} K^{-1}); L is the lining height of the furnace wall (m); d_1 is the radius of the large crucible (m); and d_2 is the radius of the furnace body (m).

The energy variation of the experimental arc furnace is nonlinear and a multistage process; however, according to the equilibrium law, the energy input of the electrode must be equal to the energy output for the entire unit and for each of its zones, as shown in Figure 8. In the figure, the arrow indicates the direction of energy transfer.
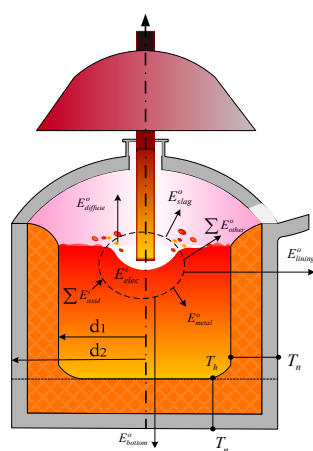
Figure 8. Schematic diagram illustrating heat exchange inside the furnace.

In the heating operation of the EAF, the actual power of the arc acting on the metal is only 60–65%; nearly 30% of the arc input power diffuses into the furnace, given by $E^o_{diffuse}$, whereas approximately 10% of the energy is used in slag heating and diffusing to the furnace bottom [2,31–33]. Theoretically, the conduction heat, E_{bottom}, can be calculated as shown in Equations (9) and (10) as:

$$E^o_{bottom} = 10\% \times E^i_{elec} - E^o_{slag} \tag{9}$$

$$E^o_{lining} = 60\% \times E^i_{elec} + \sum E^i_{oxid} - E^o_{metal} - \sum E^o_{other} \tag{10}$$

where

E^i_{elec}: amount of electrical energy in an DC-EAF.
E^o_{slag}: energy of slag before tapping.
ΣE^i_{oxid}: chemical energy of the oxidation reactions.

E_{metal}^o: enthalpy of liquid metal before tapping.

ΣE_{other}^o: other energy lost (dust, spatter, gas).

Input energy components (unit: kWh):

1. Electrical energy

The electrical energy input can be calculated based on the theoretical design of the current and voltage elements of the furnace using Equation (11):

$$E_{elec}^i = UI \times t \tag{11}$$

where U is the average input voltage of the electrode (V), assuming the laboratory allowable voltage is 40 V; I is the average input current of the electrode (A), assuming the laboratory allowable current is 500 A; and t is time duration for which the furnace is operated (h), t = 90 min.

2. Chemical energy of element reactions

After melting of titanium-containing metal pellets, titanium enters the slag in the form of oxide, and metal iron and partially reduced ferrous oxide form the metal molten pool. [2], as described by Equations (12)–(17):

$$[C] + [O] = \{CO\} \tag{12}$$

$$[C] + 2[O] = \{CO_2\} \tag{13}$$

$$C + 2FeO = 2Fe + CO_2 \tag{14}$$

$$Cr_2O_3 + 3C = 2Cr + 3CO \tag{15}$$

$$C + 2V_2O_5 = 4VO_2 + CO_2 \tag{16}$$

$$FeTiO_3 + C = TiO_2 + Fe + CO \tag{17}$$

The heat generated from the chemical reaction mainly includes the heat generated by the elemental reaction in the bath, which can be calculated using Equation (18):

$$E_{element}^i = m(Y_i - X_i)Q_{i-o} \tag{18}$$

where m is the mass of the metal inside the crucible (kg), Y_i is the concentration of C, Cr, Fe, and other elements in the raw materials (%), X_i is the concentration of C, Cr, Fe, and other elements in the product (%), and Q_{i-o} is the heat released (KJ/kg), by the oxidation of C, Cr, Fe, and other elements, per kilogram.

Similarly, dust oxidation also produces a small amount of energy; 77% of Fe in the dust is oxidized to FeO, and 22% of Fe is oxidized to Fe_2O_3 [2], which can be calculated by Equation (19):

$$E_{other}^i = m\left(77\% \times Q_{Fe-FeO} \times 56/72 + 22\% \times Q_{Fe-Fe_2O_3} \times 112/160\right) \times 1.6\% \tag{19}$$

where m is the mass of the metal inside the crucible (kg), Q_{Fe-FeO} is the energy released during the oxidation of Fe into FeO (KJ/kg), $Q_{Fe-Fe_2O_3}$ is the energy released during the oxidation of Fe into Fe_2O_3 (KJ/kg), and 1.6% is the proportion of dust in the total metal.

Output energy components (unit: kWh):

1. Energy of liquid metal before tapping

This part is calculated using ilmenite pellets as the raw material for EAF smelting. Before melting to form liquid metal, it must absorb some energy, which can be calculated by Equation (20):

$$E_{metal}^o = m(c_s(T_m - T_r) + c_l(T_h - T_m) + Q_{lh}) \tag{20}$$

where m is the mass of the metal inside the crucible (kg), c_s is the solid heat capacity of liquid metal J/(kg·K); T_m is the melting point of liquid metal (K); T_r is the raw material

temperature, $T_r = 302$ K; c_l is the liquid heat capacity of liquid metal J/(kg·K); T_h is the temperature during tapping, $T_h = 1923$ K; and Q_{lh} is the latent heat of melting of ilmenite (KJ/kg).

2.   Energy of slag at tapping

This is equivalent to the enthalpy of the formation of the final slag at the tapping temperature. The total amount of slag is, on an average, equal to 6–7% of the mass of the liquid metal [2], which becomes evident from Equation (21):

$$E_{slag}^o = m\left(c_{slag}(T_h - T_r) + Q_{slag-lh}\right) \times 6\% \tag{21}$$

where m is the mass of the metal inside the crucible (kg), T_h is the temperature during tapping; $T_h = 1923$ K; T_r is the temperature of the added raw material, $T_r = 302$ K; $Q_{slag-lh}$ is the latent heat of slag (KJ/kg); and c_{slag} is the solid heat capacity of the slag J/(kg·K).

3.   Other energy losses

The energy, E_{splash}^o, lost due to splashing, about 8% of the liquid metal energies, and the energies, E_{ib}^o, E_{dust}^o, E_{gas}^o, carried away by the iron beads, dust, and gas escaping through the furnace door and electrode gap, respectively, must also be considered in the calculations. The total amount of dust is, on an average, equal to 2% of the liquid metal [2]. It is assumed that the average temperature of the flue gas is 1723 K. All these parameters can be calculated by Equations (22)–(25).

$$E_{splash}^o = 0.8\% \times E_{metal}^o \tag{22}$$

$$E_{ib}^o = m_{ib}\left(c_{s-ib} \times \left(T_f - T_r\right) + c_{l-ib} \times \left(T_h - T_f\right) + Q_{ib-lh}\right) \tag{23}$$

$$E_{dust}^o = m((1450 - T_r) + Q_{dust-lh}) \times 2\% \tag{24}$$

$$E_{gas}^o = m_{gas} \times c_{gas} \times (1450 - T_r) \tag{25}$$

where m is the mass of the metal inside the crucible (kg), m_{ib} is the mass of the Fe beads (kg); c_{s-ib} is the solid heat capacity of the Fe beads J/(kg·K); c_{l-ib} is the liquid heat capacity of the Fe beads J/(kg·K); T_r is the temperature of the raw material, $T_r = 302$ K; T_f is the melting point of Fe, $T_f = 302$ K; Q_{ib-lh} is the latent heat of the Fe beads (KJ/kg); $Q_{dust-lh}$ is the latent heat of dust (KJ/kg); m_{gas} is the mass of the gas (kg); and c_{gas} is the gaseous heat capacity of the furnace gas J/(kg·K).

$$E_{elec}^i + \sum E_{oxid}^i = E_{metal}^o + E_{slag}^o + \sum E_{other}^o + E_{bottom}^o + E_{diffuse}^o + E_{lining}^o \tag{26}$$

The energy balance formula is shown in Equation (26), and the energy balance, calculated based on the data and the above-mentioned equations, is shown in Table 2.

Based on the calculated lining thickness, an appropriate refractory material is selected according to the actual insulation effect. The lining material of an electric furnace should be highly fire resistant and have good thermal stability and low thermal conductivity. It is more economical to select high-quality refractories and use thinner linings to ensure that heat loss is not reduced [34]. The lining mainly consists of a thermal insulation layer, protective layer, and working layer. The parameters of the commonly used refractory materials are listed in Table 3 [35].

Table 2. Energy balance of DC-EAF.

Input Energy		kWh (10 kg)$^{-1}$	%
1. Electric energy	E_{elec}^i	15	96.22
2. Chemical energy of oxidation reactions	$\sum E_{oxid}^i$	0.59	3.78
energy of element oxidation	$E_{element}^i$	0.44	2.82
other small energy sources	E_{other}^i	0.15	0.96
-	-	Σ 15.59	100

Table 2. *Cont.*

Output energy		kWh (10 kg)$^{-1}$	%
1. Energy of liquid metal before tapping	E^o_{metal}	3.82	24.50
2. Energy of slag before tapping	E^o_{slag}	0.22	1.41
3. Other energy losses	$\sum E^o_{other}$	0.14	0.90
energy of the splash	E^o_{splash}	0.03	0.19
energy carried away by the iron beads	E^o_{ib}	0.01	0.07
energy carried away by the dust	E^o_{dust}	0.07	0.45
energy taken away by the gas	E^o_{gas}	0.03	0.19
4. Energy diffused at the bottom	E^o_{bottom}	1.28	8.21
5. Energy diffused in the furnace	$E^o_{diffuse}$	4.5	28.87
6. Loss of energy from furnace walls	E^o_{lining}	5.63	36.11
-	-	Σ 15.59	100

Table 3. Main parameters of the refractory materials.

Materials	Temperature T/°C	Density ρ/(kg m^{-3})	Thermal Conductivity λ/(W m^{-1} °C^{-1})
Asbestos board	600–700	80–140	0.10–0.26
Diatomite	900	440–500	0.0395 + 0.00019 T
Fireclay	1100–1300	800–1300	[0.29–0.41] + 0.00026 T
Fireclay brick	1350–1450	1800–2040	[0.7–0.84] + 0.00058 T
Magnesia brick	600–1700	2300–2600	2.1 + 0.00019 T

The insulation layer of the furnace lining was made of asbestos board, and the thickness was approximately 10 mm. The upper asbestos board was covered with a layer of diatomaceous earth, with a thickness ranging from 5 to 20 mm. Another layer of clay bricks was built at the bottom and side-wall of the furnace, and the cracks were filled with clay powder and compacted. A conductive plate was placed on top of the firebricks at the bottom, surrounded by clay powder, and a rectangular graphite plate, dusted with graphite powder, was laid on top. The furnace walls were lined with magnesia bricks and filled with clay powder. The roof of the furnace was casted with a refractory material. The furnace lining structure is shown in Figure 9.
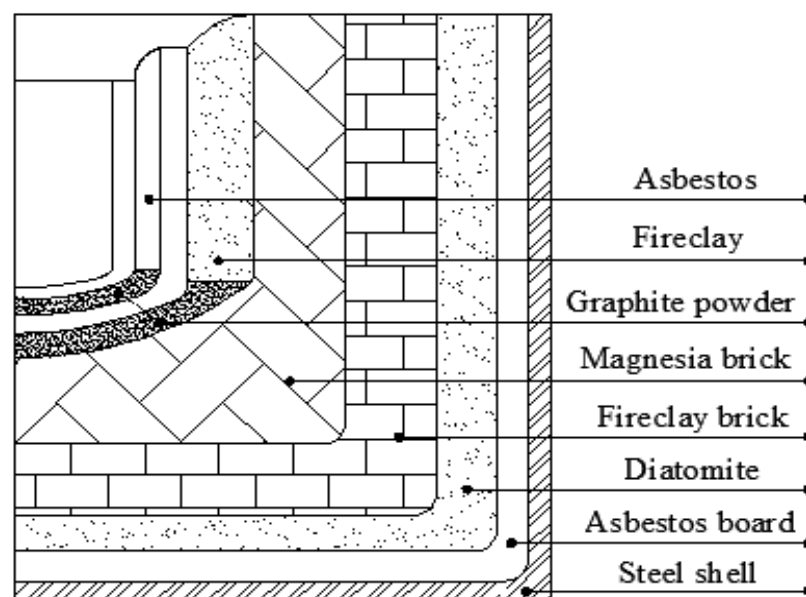

Figure 9. Illustration of the furnace lining with refractory materials.

Thus, the diameter of the furnace body can be calculated by considering all the above-mentioned refractory material layers as:

$$D_{body} = D + 2\delta + 2\varepsilon + 2\beta \qquad (27)$$

where D_{body} is the diameter of the furnace body (m), D is the inner diameter of the crucible, δ is the thickness of the lining, ε is the thickness of the crucible, and β is the thickness of the steel shell (6 to 32 mm).

2.3. Overall Design of the Electric Furnace

The DC-EAF system consists of transformers, rectifiers, EAFs, control cabinets, coolers, cyclones, etc. According to the actual situation, we chose a three-phase oil-immersed transformer, with a bridge rectifier, to obtain the direct current required by the EAF. The main parameters of the EAF transformer are listed in Table 4.

Table 4. Main parameters of the furnace transformer.

Items	Parameters	Items	Parameters
Connection Mode	Triangle/Star	Rectifier Mode	Bridge Rectifier
Input voltage	380 V	Direct voltage output	35/40/45/50 V
Input current	75 A	Direct current output	≤1250 A

The lining and bottom thicknesses and other dimensions of the furnace are shown in Table 5.

Table 5. Furnace structure parameters and corresponding dimensions.

Items	Parameters	Items	Parameters
Electrode Diameter	40 mm	Stroke of Electrode	1000 mm
Reaction chamber height (H_1)	90 mm	Small crucible thickness	20 mm
Small crucible diameter (dr)	165 mm	Large crucible thickness	25 mm
Large crucible diameter (Dr)	255 mm	Small crucible height (h)	50 mm
Furnace top height (h_3)	130 mm	Large crucible height (H)	70 mm
Furnace bottom thickness	330 mm	Furnace lining thickness	265 mm
Furnace body height	750 mm	Furnace body diameter	800 mm

The transformer and the electrode are connected by two flexible water-cooled cables, which allow the electrodes to move vertically and swing with the furnace body. The dust removal equipment was designed according to the size of the DC-EAF. The furnace is shown schematically in Figure 10.
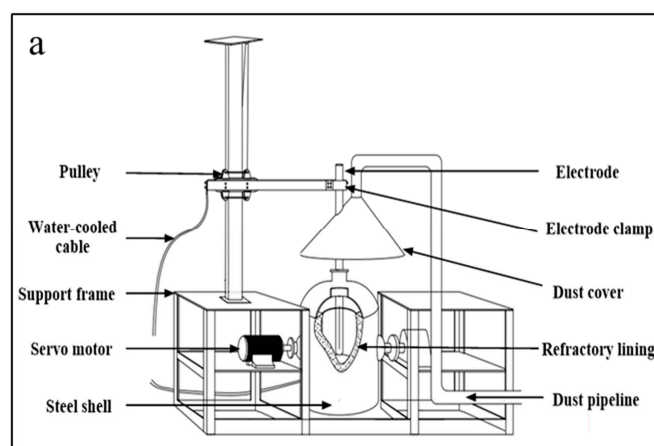

Figure 10. *Cont.*

Figure 10. (**a**) Schematic diagram and (**b**) image of the electric arc furnace.

The designed DC-EAF can be used to smelt metal and slag. This DC-EAF enables rapid melting with good heat preservation; however, some limitations have been observed in the designed DC-EAF-induced smelting, namely, the electrical parameters of the electrode cannot be controlled easily, which leads to arc breaking, excessive electrode consumption, long smelting time, high power consumption, and high cost of single furnace smelting.

3. Data Collection and Applications

As an effective approach to solve the problem of excessive power consumption, we designed a real-time process monitoring system by analyzing the relationship between the current and the arc, based on the DC arc model. This system collects information pertaining to the electrical parameters (electrode voltage, electrode current, etc.) in real time via PLC, which guides the operation of power supply in the experiment and collects feedback in real time. The monitoring system is driven by the information flow to realize closed-loop control of the smelting process effectively.

3.1. Data Collection

During the EAF smelting process, the arc length has a significant effect on the heat transfer efficiency of the liquid metal [36]. The arc length is different during each smelting period. To ensure the effective utilization of arc energy, changes in the electrode voltage and current must be monitored, and the electrode rise and fall must be adjusted reasonably, as directed by Equation (28):

$$l = \frac{K_T \times I^2}{9.8\mu \times S} + H \tag{28}$$

where l is the arc length (m); H is the distance from the bottom of the electrode to the liquid metal level (m); K_T is the correction coefficient (N/kA^2); I is the arc current (kA); μ is the density of liquid metal; and S is the area of arc impact (m^2).

The electrical parameters of each stage of the smelting process are collected and stored in the SQL2008 database for subsequent processing and analysis.

3.2. Software Development

To shorten the data acquisition time, while simultaneously ensuring collection accuracy, KEPServerEX software was used to configure the data collection environment. The software is widely used, owing to its simple operation and fast data processing speed.

The software was developed using Visual Studio.NET 2010 software by C# language. The graphical user interface (GUI) of this system is shown in Figure 11.
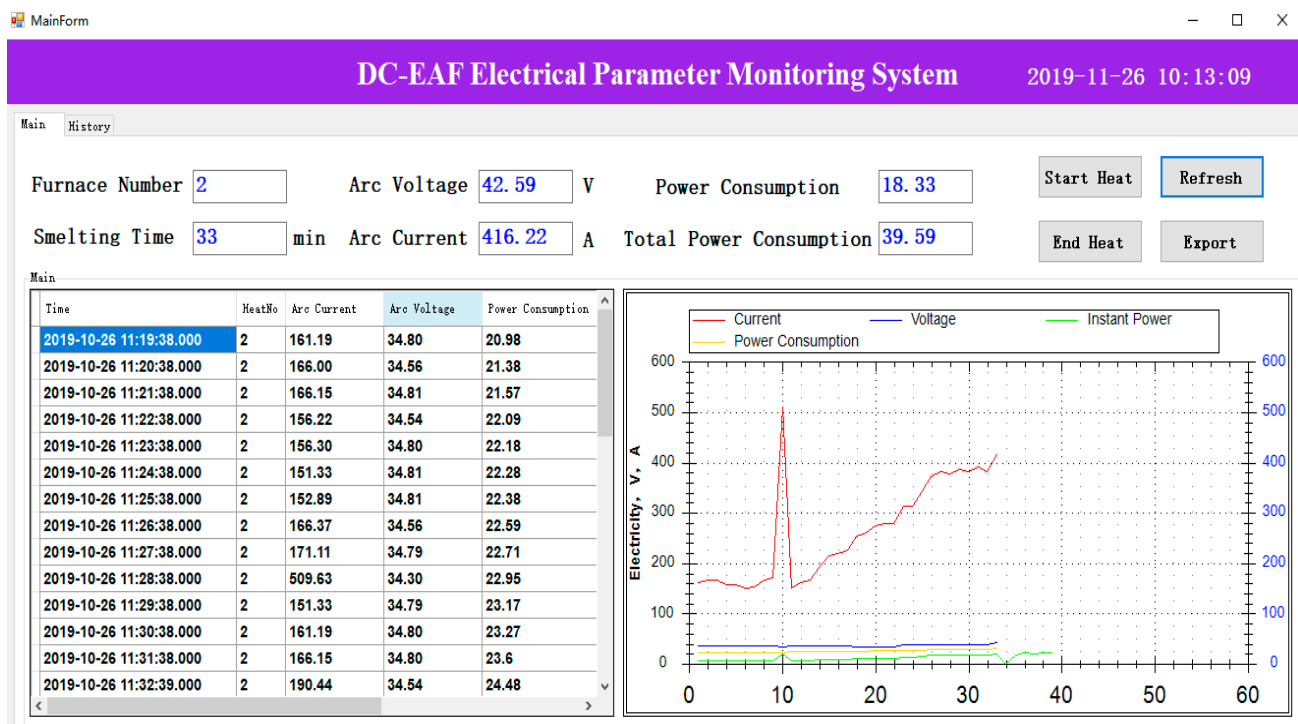
Figure 11. GUI for the process monitoring system.

4. Results and Discussion

To evaluate the operation and performance of the designed DC-EAF, titanium-containing metallized pellets were used for melting test verification. The content of Cr_2O_3, V_2O_5 and other impurities in titanium-containing metallized pellets was high. Adding reducing agent during the melting process can result in some impurities to reduce and enter the molten iron, thus reducing the impurity content in high-titanium slag, improving the alloy elements in molten iron, and realizing the separation of high-titanium slag and iron. The raw materials were detected by X-ray fluorescence spectroscopy (XRF), the composition of the metallized pellets and coke is shown in Tables 6 and 7.

Table 6. Composition of high-titanium metal pellets (wt.%).

Composition	Fe	CaO	SiO₂	MgO	Al₂O₃	K₂O	Na₂O	Cr₂O₃	TiO₂	V₂O₅
Content	65.66	0.39	2.19	0.64	1.59	0.073	0.17	0.58	26.10	0.41

Table 7. Coke composition (wt.%).

Composition	C	O	Al	Si	S	Fe	Ca	Mg	Ti	Cr
Content	89.10	5.45	1.67	1.64	1.12	0.32	0.23	0.16	0.05	<0.01

Titanium-containing metallized pellets were crushed to 10–15 mm by the counter-roller crusher. To find the optimal concentration of the reducing agent, four groups of experiments were conducted with coke concentrations (wt.%) of 0, 1, 4, and 6% coke, respectively. It was estimated that the experimental temperature of each group reached 1600 °C and the melting time was 90 min. Figure 12 illustrates the physical schematics of the reduced samples and crucibles in the four groups of experiments. The cross-section of the crucible reflects the clear boundary between metal and slag, which effectively prevents secondary pollution between the metal and slag.
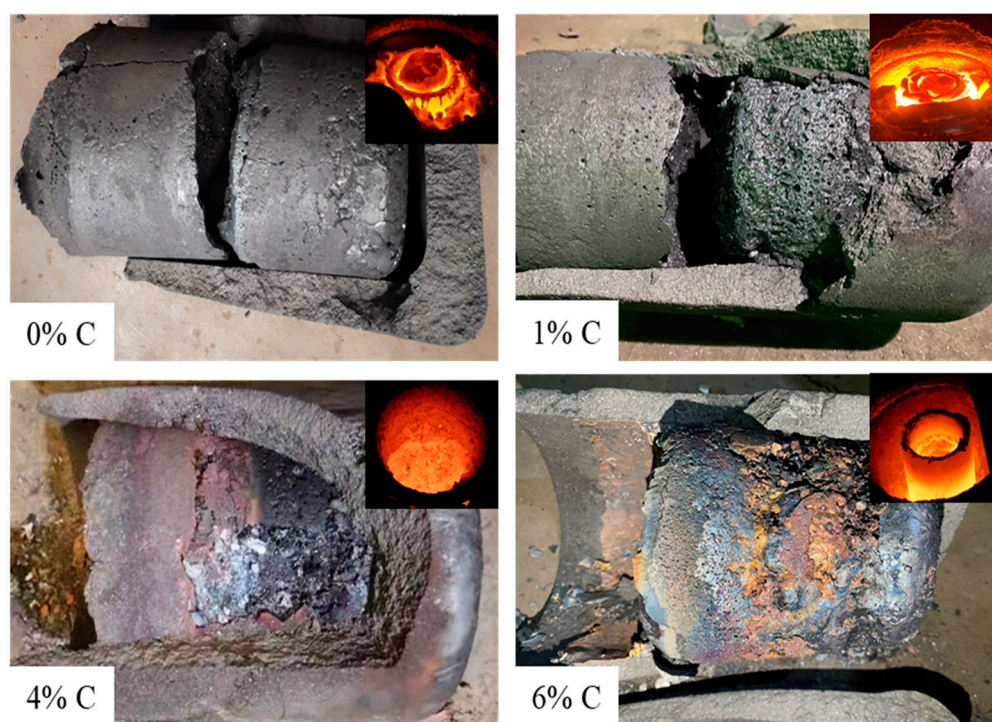
Figure 12. Physical schematic of the reduced samples and crucible.

The reduced slag sample was ground into powder, and visible metallic iron particles were screened out. Then iron was separated from titanium slag by a wet magnetic method. The titanium slag before and after wet magnetic separation was analyzed by chemical element titration. The results are shown in Table 8.

Table 8. Composition of coke samples (wt.%).

NO.	Pellet Weitght (kg)	Coke Weight (kg)	Time (min)	Temperature (°C)	Content in Slag after Smelting			
					FeO (%)	TiO_2 (%)	Cr_2O_3 (%)	V_2O_5 (%)
1	6	0	90	1841	19.35	59.44	1.29	1.14
2	12	0.12	90	1620	14.54	65.45	0.56	1.57
3	12	0.48	90	1607	3.04	93.34	0.31	0.47
4	12	0.72	90	1594	11.88	86.83	0.25	0.30

Table 8 shows that without coke, the TiO_2 content in slag was 59.44%, and the Cr_2O_3 content in slag was 1.29%. When the coke with a total weight of 1% was added, the TiO_2 content in the slag was 65.45%, and the Cr_2O_3 content in the slag was 0.56%. When coke with a total weight of 4% was added, TiO_2 in slag was 93.34%, and Cr_2O_3 in slag was 0.31%. When coke with a total weight of 6% was added, the TiO_2 content in the slag was 86.83%, and the Cr_2O_3 content in the slag was 0.25%. These results demonstrate that coke with a total weight of 4% was the effective condition for facilitating the enrichment effect of TiO_2 in high-titanium slag, with TiO_2 in slag reaching 93.34%. This test verifies the applicability of the designed DC electric arc furnace, highlighting its potential applicability in industry.

In future studies, the influence of the distance between electrodes and the molten steel on the EAF performance must be investigated to improve the monitoring system and extend its applications.

5. Conclusions

Herein, the development of EAF over the years was reviewed and analyzed, whereby it was demonstrated that the existing EAFs should be improved via mitigation of their

drawbacks (incomplete separation of metal and slag and poor thermal insulation effect) and redesigned through experimentation in universities and research institutes. Based on these points, in this study, we developed a DC-EAF that was capable of fast heating and producing a good separation effect between the metal and slag. The main conclusions of our study are as follows:

1. The mechanical structure was designed, which included the power supply mode, electrode and electrode holder, electric circuit, crucible, and the reaction chamber structure. The embedded design of the crucible was used to separate the metal and the slag. In addition, the surface lining and bottom thicknesses were determined using the heat balance equations.
2. The EAF smelting efficiency factors were analyzed. The voltage, current, smelting time, and temperature data of the experimental electrode were collected by PLC, and the electric parameter monitoring system of the DC-EAF was developed.
3. In the performance evaluation test of the arc furnace, the optimal weight percentage of the reducing agent was investigated. The results show that for separating 12 kg of titanium-containing metallized pellets when the temperature (1607 $^\circ$C) and smelting time (90 min) were constant, coke with a total weight of 4% coke was the most effective condition for facilitating the enrichment effect of TiO_2 in high-titanium slag; consequently, the TiO_2 content in slag reached 93.34%. This shows that the proposed DC-EAF meets the design requirements of lining thickness and achieves a good metal-slag separation.

Author Contributions: B.X., L.Y. contributed to the conception of the study; B.X. performed the experiment; S.W., F.Z. contributed significantly to analysis and manuscript preparation; B.X., Z.Y. performed the data analyses and wrote the manuscript; Y.G., F.C., L.Y. helped perform the analysis with constructive discussions. All authors have read and agreed to the published version of the manuscript.

Informed Consent Statement: Not applicable.

Data Availability Statement: Restrictions apply to the availability of these data. Data was obtained from Central South University and are available from the Botao Xue with the permission of Central South University.

Conflicts of Interest: The authors declare no conflict of interest.

References

1. Madias, J. *Treatise on Process Metallurgy*; Seetharaman, S., Ed.; Elsevier: Boston, MA, USA, 2014; pp. 271–300.
2. Toulouevski, Y.N.; Zinurov, I.Y. *Innovation in Electric Arc Furnaces II: Scientific Basis for Selection*; Toulouevski, Y.N., Zinurov, I.Y., Eds.; Springer: Berlin/Heidelberg, Germany, 2013; pp. 1–24.
3. Ministry of Industry and Information Technology of the People's Republic of China. The Ministry of Industry and Information Technology Issued a Notice on the Steel. Industry Adjustment and Upgrading Plan (2016–2020). Available online: https://www.miit.gov.cn/zwgk/zcwj/wjfb/zh/art/2020/art_4ec2537d42b947e3bbac6a70babbaa05.html (accessed on 14 November 2016).
4. Lupi, S. *Fundamentals of Electroheat: Electrical Technologies for Process Heating*; Lupi, S., Ed.; Springer International Publishing: Cham, Switzerland, 2017; pp. 83–205.
5. Xu, X. Overview of the development of DC arc furnaces at home and abroad. *Hum. Metall* **1996**, *2*, 57–60.
6. Yu, M.Q. Overview of the development of DC arc furnace technology at home and abroad. *Shanghai Metall Inf.* **1998**, *4*, 1–10.
7. Oyawale, F.A.; Olawale, D.O. Design and prototype development of a mini-electric arc furnace. *Pac. J. Sci. Technol.* **2007**, *8*, 12–16.
8. Yin, J.F. Experimental study on process granulated water quenching slag by dc electric arc furnace. *Min. Metall* **2011**, *20*, 82–85.
9. Barbouche, M.; Hajji, M.; Ezzaouia, H. Electric arc furnace design and construction for metallurgical and semiconductor research. *Int. J. Adv. Manuf. Technol.* **2016**, *82*, 997–1006. [CrossRef]
10. Sun, D.C.; Sun, Y.C. Current Situation and Development of DC Arc Furnace at Home and Abroad. In Proceedings of the 9th Academic Conference on Carbon Materials, Chinese Society of Metals, Shanghai, China, 1 April 1994.
11. Schub, M.; Xiao, B. Economical and energy-saving unarc DC arc furnace. *Energy Metall Ind.* **1993**, *12*, 57–60.

12. Gu, H.X. Direct current electric arc furnace. *Spec. Steel.* **1983**, *4*, 88–90.

13. Zhang, H.S. Reconstruction of 5—ton arc furnace. *Heavy Mach.* **1989**, *4*, 47–48.

14. Wang, J.Z.; Liu, X.W. Research and development of DC arc furnace in Chengdu Seamless Steel. Tube Company. *Spec. Steel. Technol.* **1995**, *1*, 23–24.

15. Liu, X.R. Design and Operation of 10t Single Electrode DC Arc Furnace. *Ind. Heat* **1995**, *2*, 33–35.

16. Sui, L.L. *Theory and Technology of Green Utilization of Titanium Slag*; Northeastern University: Boston, MA, USA, 2015.

17. Ma, X.; Han, F.X.; Lei, T. Factor of reductant carbon during titanium slag smelting in closed direct current arc furnace. *J. Kunming Univ. Technol.* **2013**, *38*, 6–10.

18. Edneral, F.P. *Electrometallurgy of Steel and Ferro-Alloys*; MIR Publishers: Moscow, Russia, 1979; pp. 1–87.

19. Bowman, B. Performance Comparison Update-Ac vs Dc Furnaces. *Iron Steel. Eng.* **1995**, *72*, 26–29.

20. Saevarsdottir, G. *Handbook of Ferroalloys*; Gasik, M., Ed.; Butterworth-Heinemann: Oxford, UK, 2013; pp. 139–175.

21. Zheng, J.H. Comparison and technology analysis of UHP electrode performance in AC and DC electric arc furnaces. *Carbon Tech.* **2002**, *4*, 28–32.

22. Yan, L.Y.; Wu, Z.T.; Rui, S.S. Design and application of the bottom electrode of DC arc furnace. *Metall. Equip.* **1995**, *05*, 16–18.

23. Mullinger, P.; Jenkins, B. *Industrial and Process. Furnaces*, 2nd ed.; Mullinger, P., Jenkins, B., Eds.; Butterworth-Heinemann: Oxford, UK, 2013; pp. 289–335.

24. Dednev, A.A.; Elizariov, K.A.; Kissel'man, M.A.; Nekhamin, S.M. Control systems of melting electric furnaces in metallurgy and mechanical engineering. *Russ. Metall* **2013**, *6*, 442–449. [CrossRef]

25. Shinya, O. Programmable Logic Controller. *Progr Log. Control.* **2012**, *62*, 1–22.

26. Skripchenko, S.V.; Nikol'skii, L.E.; Pis'mennyi, V.A. Study of the efficiency of use of electric power in the production of steel in an arc furnace. *Metall* **1988**, *32*, 150–151. [CrossRef]

27. Siemens. S7-200 Programming Manual. Available online: https://cache.industry.siemens.com/dl/files/582/1109582/att_22063/v1/s7200_system_manual_en-US.pdf (accessed on 10 February 2021).

28. Postel, J. DOD standard transmission control protocol. *ACM SIGCOMM Comput. Commun. Rev.* **1980**, *10*, 52–132. [CrossRef]

29. IEEE. *National Electrical Safety Code (NESC) Handbook*, 7th ed.; IEEE: Piscataway Township, NJ, USA, 2011; pp. 1–802.

30. Allen, L. Clapp. Installation and Maintenance of Equipment. In *NESC Handbook: A Discussion of the National Electrical Safety Code*; IEEE: Piscataway Township, NJ, USA, 2011; pp. 148–176.

31. Persson, J.A.; Andrews, R.E.; Maola, M. Arc Furnace Electrode Control. US US4620308 A, 28 October 1986. Available online: https://www.freepatentsonline.com/4620308.pdf (accessed on 10 February 2021).

32. Dong, Q.; Zhang, J. Simulation of superfluid and heat transfer in plasma arc region of AC electric arc furnace. In *CFD Modeling and Simulation in Materials Processing*; Nastac, L., Zhang, L., Thomas, B.G., Zhu, M., Ludwig, A., Sabau, A.S., Pericleous, K., Combeau, H., Eds.; John Wiley & Sons, Inc.: Hoboken, NJ, USA, 2016; pp. 35–42.

33. Reynolds, Q.G.; Jones, R.T.; Reddy, B.D. Mathematical and computational modelling of the dynamic behaviour of direct current plasma arcs. *J. S. Afr. Inst. Min. Metall.* **2010**, *110*, 733–742.

34. Biswas, S.; Sarkar, D. *Introduction to Refractories for Iron- and Steelmaking*; Biswas, S., Sarkar, D., Eds.; Springer International Publishing: Cham, Switzerland, 2020; pp. 249–267.

35. Song, X.W. *Technology of Refractory Materials*; Beijing Chemical Industry Press: Beijing, China, 2008; pp. 63–105.

36. Kazak, O. Modeling of vortex flows in direct current (DC) electric arc furnace with different bottom electrode positions. *Metall Mater. Trans. B* **2013**, *44*, 1243–1245. [CrossRef]